Saxitoxin Is a Gating Modifier of hERG K^+ Channels

Jixin Wang, Joseph J. Salata, and Paul B. Bennett

Department of Molecular Pharmacology, Merck Research Laboratories, West Point, PA 19486

ABSTRACT Potassium (K^+) channels mediate numerous electrical events in excitable cells, including cellular membrane potential repolarization. The hERG K^+ channel plays an important role in myocardial repolarization, and inhibition of these K^+ channels is associated with long QT syndromes that can cause fatal cardiac arrhythmias. In this study, we identify saxitoxin (STX) as a hERG channel modifier and investigate the mechanism using heterologous expression of the recombinant channel in HEK293 cells. In the presence of STX, channels opened slower during strong depolarizations, and they closed much faster upon repolarization, suggesting that toxin-bound channels can still open but are modified, and that STX does not simply block the ion conduction pore. STX decreased hERG K^+ currents by stabilizing closed channel states visualized as shifts in the voltage dependence of channel opening to more depolarized membrane potentials. The concentration dependence for steady-state modification as well as the kinetics of onset and recovery indicate that multiple STX molecules bind to the channel. Rapid application of STX revealed an apparent "agonist-like" effect in which K^+ currents were transiently increased. The mechanism of this effect was found to be an effect on the channel voltage-inactivation relationship. Because the kinetics of inactivation are rapid relative to activation for this channel, the increase in K^+ current appeared quickly and could be subverted by a decrease in K^+ currents due to the shift in the voltage-activation relationship at some membrane potentials. The results are consistent with a simple model in which STX binds to the hERG K^+ channel at multiple sites and alters the energetics of channel gating by shifting both the voltage-inactivation and voltage-activation processes. The results suggest a novel extracellular mechanism for pharmacological manipulation of this channel through allosteric coupling to channel gating.

KEY WORDS: ion channel • neurotoxin • kinetic model • antiarrhythmic • pro-arrhythmia

INTRODUCTION

The human ether-à-go-go–related gene (hERG)* potassium (K^+) channel has been discovered recently to play important roles in excitable tissues. hERG channels (Warmke and Ganetzky, 1994; Trudeau et al., 1995) play a role in myocardial repolarization (Sanguinetti et al., 1995; Spector et al., 1996; Wang et al., 1998) and are associated with both the congential (inherited) and the acquired (drug induced) long QT syndromes (LQT2) that may cause fatal cardiac arrhythmias. hERG K^+ channels are an unusually promiscuous drug target through internal pore blockade (Sanguinetti et al., 1995; Mitcheson et al., 2000), and are especially sensitive to external cations, e.g., Ca^{2+} and Cd^{2+}, which act as a gating modifiers (Ho et al., 1998; Anumonwo et al., 1999; Johnson et al., 1999a,b; Po et al., 1999; Sanchez-Chapula and Sanguinetti, 2000). Organic molecules as hERG gating modifiers have not been described. Saxitoxin (STX) is a neurotoxin found in clams and mussels that have fed on members of the genus *Gonyaulax* and related dinoflagellates whose local population explosions are associated with a red tide (Kao and Nishiyama, 1965; Kao 1966; Narahashi et al., 1967; Chiba and Hashimoto, 1969; Evans, 1969; Kao 1972; Wong et al., 1971; Narahashi, 1972; Henderson et al., 1973). STX is a complex guanidine-based alkaloid with potent biological activity. It inhibits voltage-gated sodium channels by binding to the outer ion conduction pore, and causes rapid neuromuscular paralysis (Campbell and Hille, 1976; Wagner and Ulbricht, 1976; Noda et al., 1989; Lipkind and Fozzard, 1994). It is, in fact, one of the most toxic nonprotein substances known. A single submilligram dose can be fatal in humans, and as such STX is 2,000 times more toxic than sodium cyanide, and 100 times more poisonous than strychnine. During the course of investigating I_{Kr} (the hERG associated K^+ current) in cardiac myocytes and using STX to inhibit the endogenous voltage–gated sodium channels, we were surprised to observe that STX appeared to affect I_{Kr}. An affect of this toxin on K^+ channels was unprecedented as STX is believed to be highly sodium channel selective.

In this paper, we address the mechanism of inhibition of this potassium channel and the nature of the interaction between STX and the hERG channel. We discovered that STX modifies hERG K^+ channel gating both by destabilizing inactivated states and through sta-

Address correspondence to Paul B. Bennett, Department of Molecular Pharmacology, WP42-200, Merck Research Laboratories, 770 Sumneytown Pike, West Point, PA 19486. Fax: 215-993-5098; E-mail: Paul_bennett@merck.com

*Abbreviations used in this paper: ErgTx, ergtoxin; hERG, human ether-à-go-go–related gene; STX, saxitoxin; TTX, tetrodotoxin.

J. Gen. Physiol. © The Rockefeller University Press • 0022-1295/2003/06/583/16 $8.00
Volume 121 June 2003 583–598
http://www.jgp.org/cgi/doi/10.1085/jgp.200308812

bilizing closed states, mechanisms that are completely distinct from the way in which STX inhibits sodium channels. Toxin-bound channels require stronger depolarization to open and they close much faster upon repolarization, indicating that STX inhibits ion flux by modifying channel gating, not by pore occlusion per se. The divalent, positively charged STX molecule also caused an increase in K^+ current under certain conditions. This apparent paradox is most simply explained by a shift in the voltage dependencies of the fundamental processes that govern activation and inactivation of this channel and the different rates of channel equilibration with these states.

MATERIALS AND METHODS

Cell Preparation for Electrophysiology

HEK-293 hERG cell lines were grown to 80% confluence, washed two times with PBS, and then trypsinized with 0.05% trypsin-EDTA (GIBCO BRL) for 2 min at 37°C, and resuspended in culture medium. Cells were studied within 8 h.

Voltage-Clamp Recording Methods

Potassium currents were recorded using the whole-cell patch clamp technique. Cells were transferred to an 80 μl recording chamber (RC-24; Warner Instrument Corp.) and superfused with a solution containing (mM): 132 NaCl, 4 KCl, 1.2 $MgCl_2$, 1.8 $CaCl_2$, 10 HEPES, 11 glucose, pH = 7.2 at a flow rate of ~1 ml/min. The temperature was maintained at 36 ± 1°C with a water-jacketed preheating system and a DC-powered heating system (Cell MicroControls). In some experiments, currents were recorded at room temperature of 23 ± 1°C. An Axopatch 200A patch clamp amplifier was connected to a desktop PC computer (Compaq DESKPRO 6000) through a Digidata 1200 interface (Axon Instruments, Inc.). Patch pipettes were fabricated from capillary glass (Kimble Products, 0.8–1.1 × 100 mm; catalog, Kimax-51) using a vertical micropipette puller (model L/M-3p-A, LIST-MEDICAL). Pipettes resistances were 2–4 MΩ when filled with a solution containing (mM): 119 K-gluconate, 15 KCl, 3.2 $MgCl_2$, 5 EGTA, 5 K_2ATP, 5 HEPES, pH = 7.35. Cell capacitance and series resistance were compensated (80–90%) before recording. Drugs and solutions were added either through whole bath perfusion or using a dual channel rapid solution change device (SF-77B Perfusion Fast Step; Warner Instruments, Inc.). Using this method, controls included changing between the same solution in each pipette.

STX was obtained from two different sources, Sigma-Aldrich (product number: S-1417, Saxitoxin and diacetate salt protogonyaulax sp., Lot no. 89H1306) and CALBIOCHEM (product number 559385, Saxitoxin, diacetate salt gonyaulax sp., Lot no. B19491 and B17901). According to the purification protocol, the concentrations of contaminant metal ions should be 0.1 μM or lower in the 1 mM STX stock solution used. The final STX purification step employed a BIO-RAD Chelex-100 resin to remove contaminant metal ions. The highest STX concentration used in this study was 10 μM. In this case, there is a 100–fold dilution of the stock solution. Thus, the highest concentration of any contaminant metal ions should be 1 nM or less.

Data Analysis

Data were acquired and analyzed using pCLAMP8 (Axon Instruments, Inc.), Origin 5.0 (Microcal Software), SigmaPlot 5.0 (SPSS, Inc.) and Microsoft Excel software. Simulations were conducted using ModelMaker v.3 (Cherwell Scientific).

Voltage-clamp Data Analysis

Channel kinetics were evaluated by fitting appropriately normalized time (t) dependent currents with exponential functions consisting of one or more terms:

$$y(t) = A_0 + \sum_{i}^{n} A_i \exp^{-t/\tau i}, \quad (1)$$

where i = 1 or 2, A_i and τ_i represent the amplitude and time constants of the i_{th} component, respectively. The fits were based on nonlinear least-squares regression methods. The goodness-of-fit was determined by minimizing residual sum of squared errors, and visual examination of the residuals and fits. Voltage dependence of channel opening was estimated by fitting a form of a Boltzmann equation:

$$I/I_{max} = [1 + \exp(V_m - V_{1/2})/k]^{-1}, \quad (2)$$

where V_m represents membrane potential, $V_{1/2}$ is the membrane potential at $I/I_{max} = 0.5$, and k is a slope factor. Alternatively, this equation written in terms of thermodynamic parameters was used:

$$I/I_{max} = \{1 + \exp^{[\Delta G_0 + V_m \cdot z/(K_B \cdot T)]}\}^{-1}, \quad (3)$$

where ΔG_0 represents a nonvoltage dependent free energy term, z represents the number of equivalent gating charges experienced by the gating voltage sensor in the membrane electrical field, e is the fundamental charge of an electron, and K_B and T are the Boltzmann constant and absolute temperature (°K), respectively.

Pharmacological Data Analyses and Statistics

Summary data are expressed as mean ± SEM. Group means were compared using an unpaired *t test* and differences were considered significant at the $P < 0.05$ level. In some cases concentration-effect data were fit with the Hill equation:

$$1 - I/I_{max} = \{[STX]^N/(EC_{50}{}^N + [STX]^N)\}, \quad (4)$$

where I is current, I_{Max} is the maximal current, EC_{50} is the 50% effective concentration of STX, and N is the Hill coefficient. We used this as an empirical tool to quantitatively analyze the concentration effect data. We do not ascribe any direct interpretation to nonunity Hill coefficients, except that they suggest complex higher order interactions.

RESULTS

STX Reduces hERG K^+ Currents

Fig. 1 demonstrates some of the various effects of STX on hERG K^+ current. Most apparent, 3 and 10 μM suppressed the current amplitude, both the outward current during the voltage step and the tail current upon the step to −70 mV. Fig. 1, A and B, shows hERG K^+ current recorded during a voltage clamp step to −40 mV. A concentration of 3 μM STX (Fig. 1 A) decreased the K^+ current by >90%. At 10 μM (Fig. 1 B) STX the current was almost completely suppressed. Fig. 1 C shows the

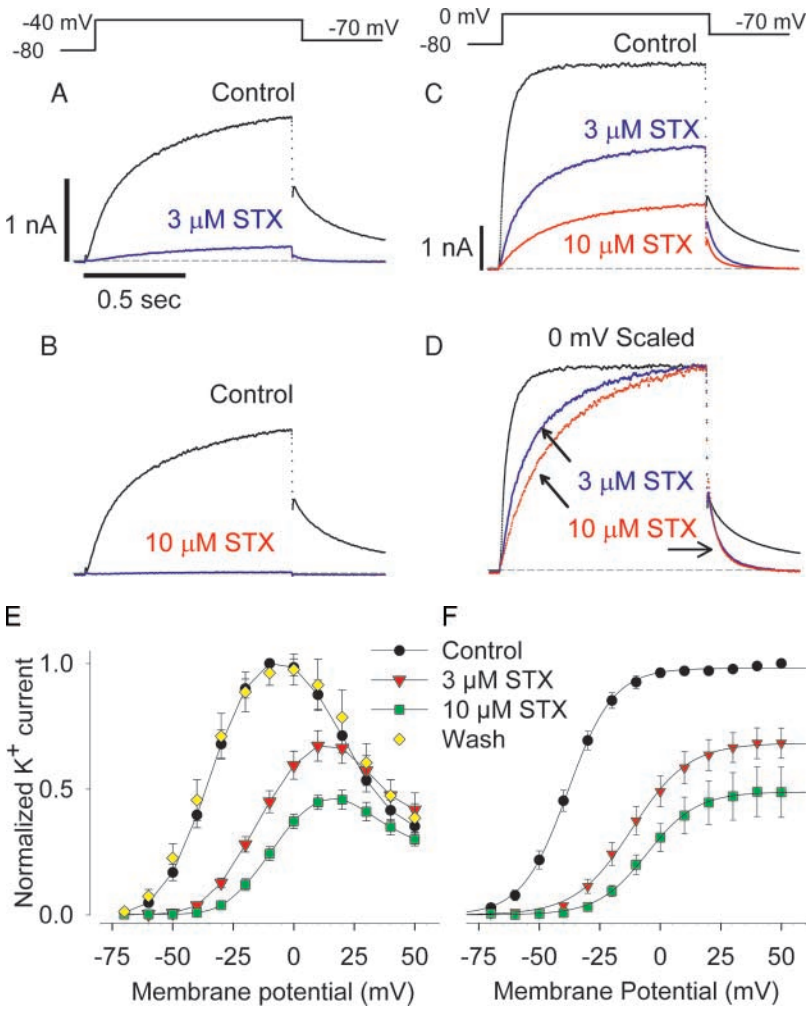

FIGURE 1. STX effects on hERG K^+ channels. hERG K^+ current traces were recorded during a voltage clamp step to either −40 (A and B) or 0 mV (C and D), followed by a step to −70 mV to record K^+ current tails. Shown are K^+ currents measured in control or during steady-state exposure to 3 and 10 μM STX. (D) Normalized K^+ currents scaled to control at the end of the voltage step to 0 mV in order to compare the kinetic changes caused by STX. (E) Voltage-activation curves where K^+ current is normalized to the maximum outward current in control. (F) Tail currents in STX normalized to the control tail maximum. Means ± SEM of from 4–6 cells.

same concentrations of STX during a step to 0 mV. The degree of suppression was less, and the kinetics of the currents were altered. The time course during the step to 0 mV was slowed, but the rate of decay of the tails was enhanced. These kinetic changes suggest that STX was still bound to the channel, but the amount of suppression was altered at 0 mV compared with −40 mV. Thus, STX appeared to increase the apparent membrane potential threshold for channel opening. In Fig. 1 D, the tracings recorded at 0 mV in 3 and 10 μM STX were normalized to the maximum outward current in control to permit comparison of the kinetics during the step and upon repolarization to −70 mV. Note that if the outward current is normalized to the control level, the peak of the tail current is the same as the control. The current reduction quickly reached its steady-state upon exposure to STX and was very rapidly reversed upon washout. The absence of tail current crossover (due to kinetic slowing) suggested that the decrease in current was not due to simple pore blockade (Armstrong, 1971). The slowing of kinetics during the voltage step and the speeding of K^+ current tails suggested a more complex mechanism. An analysis of some of the kinetic changes is summarized in Tables I and II. At −20 mV, STX increased

TABLE I

The Effect of STX on the hERG Current Activation Time Constants at −20 mV (36°C)

	Activation (V_{test} = 20 mV)						
STX (μM)	Control	0.1	0.3	1	3	10	Wash
τ_{Fast} (ms)	53 ± 7 (16)	43 ± 4 (6)	67 ± 9 (9)	101 ± 20 (8)[a]	104 ± 20 (6)[a]		50 ± 6 (7)
τ_{Slow} (ms)	310 ± 40 (16)	272 ± 34 (6)	397 ± 61 (9)	608 ± 127 (8)[a]	549 ± 63 (8)[a]	628 ± 250 (5)[a]	285 ± 38 (7)
$A_{Fast}/(A_{Fast} + A_{Slow})$	0.6 ± 0.03 (16)	0.6 ± 0.03 (6)	0.5 ± 0.03 (9)[a]	0.3 ± 0.04 (8)[a]	0.2 ± 0.06 (8)[a]	0 (5)[a]	0.6 ± 0.04 (7)

[a]Significant difference between control and STX $P < 0.05$ (number of cells).

TABLE II

The Effect of STX on the hERG Current Deactivation Time Constants (36°C)

	Deactivation (V_{test} = 50 mV and V_{tail} = −70 mV)						
STX (μM)	Control	0.1	0.3	1	3	10	Wash
τ_{Fast} (ms)	84 ± 7 (14)	47 ± 7 (4)[a]	55 ± 12 (7)[a]	60 ± 11 (5)	50 ± 7 (7)[a]	27 ± 4 (5)[a]	83 ± 8 (6)
τ_{Slow} (ms)	458 ± 32 (14)	278 ± 42 (4)[a]	250 ± 45 (7)[a]	219 ± 30 (5)[a]	173 ± 26 (7)[a]	110 ± 20 (5)[a]	110 ± 20 (5)[a]
$A_{Fast}/(A_{Fast} + A_{Slow})$	0.6 ± 0.02 (14)	0.7 ± 0.02 (4)[a]	0.6 ± 0.04 (7)	0.7 ± 0.04 (5)[a]	0.6 ± 0.03 (7)	0.7 ± 0.04 (5)[a]	0.5 ± 0.03 (6)

[a]Significant difference between control and STX $P < 0.05$ (number of cells).

both fast- and slow-time constants of the activation gating and decreased the proportion of the fast component (Table I). Fig. 1 D illustrates that STX accelerates the deactivation gating kinetics. At −70 mV after a 50-mV test pulse, STX significantly decreases both fast- and slow-time constants of the deactivation gating but increases the fraction of the fast component (Table II). These effects are opposite to the STX effects on activation gating kinetics (Table I).

Fig. 1, E and F, summarizes pooled data. The effects of STX on outward K^+ current at different membrane potentials are shown for control and 3 or 10 μM. These data reveal that STX shifted the voltage-activation process in a concentration-dependent manner and this effect was fully reversible upon washout of STX. The reduction of steady-state outward K^+ current (Fig. 1 E) by STX was greater at membrane potentials less than 0 mV. This change in the I-V curve by STX results in a larger percent inhibition at negative potentials than at positive ones (Fig. 1 E). The membrane potential "threshold" for channel opening was increased in the presence of STX, requiring greater depolarization to open the same fraction of channels.

Concentration Dependence of STX Effects

Fig. 2 A shows the change in tail current amplitudes (recorded at −70 mV) after different test potential steps in varied STX concentrations. These data were plotted as concentration-effect curves and were fit with the Hill equation (Eq. 4). The apparent potency (EC_{50}) and the Hill coefficient varied with membrane potential. The EC_{50}s ranged between 5.6 μM at +50 mV and 290 nM at −40 mV. The fitted Hill coefficient, an indicator of possible cooperativity, ranged from <1 (50 mV) to nearly 3 (−40 mV).

The effects of STX on the voltage-activation relationship of the channels were examined as shown in Fig. 2 B. Here tail currents are normalized to the maximum tail current amplitudes after a test step to 50 mV. The curves were fitted with a Boltzmann equation. STX appeared to stabilize closed states of the channel in a concentration dependent fashion. At the highest concentration tested (10 μM), the closed states were stabilized by 3.1 kcal/mol as reflected by a 33 mV shift in the channel voltage-activation relationship. These shifts were fully and rapidly reversed upon washout of STX.

STX Is not a Channel-pore Blocker

These results suggested a complex mechanism for STX, and the apparent effects on gating suggested that it was not working by a mechanism similar to that seen with sodium channels, i.e., STX did not seem to behave like a typical channel-pore blocker. To characterize the mechanisms further, we conducted experiments such

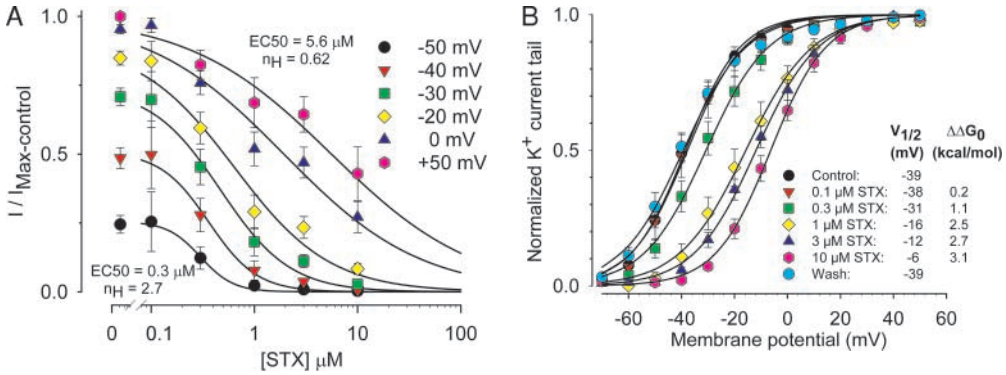

FIGURE 2. Concentration dependence of suppression of hERG K^+ currents at different membrane potentials. hERG K^+ currents were normalized to control before STX exposure at the membrane potential indicated. Data were fit with the Hill equation to estimate an EC_{50} and a Hill slope. (B) Voltage activation curves from peak tail currents. Outward tail currents measured at −70 mV after a voltage clamp step to the potential indicated were normalized to unity and fit with the Boltzmann equation to estimate the membrane potential for half maximal activation of the channels, and the energetic cost of opening the channels in the presence of different concentrations of STX. Full recovery was observed upon washout of STX.

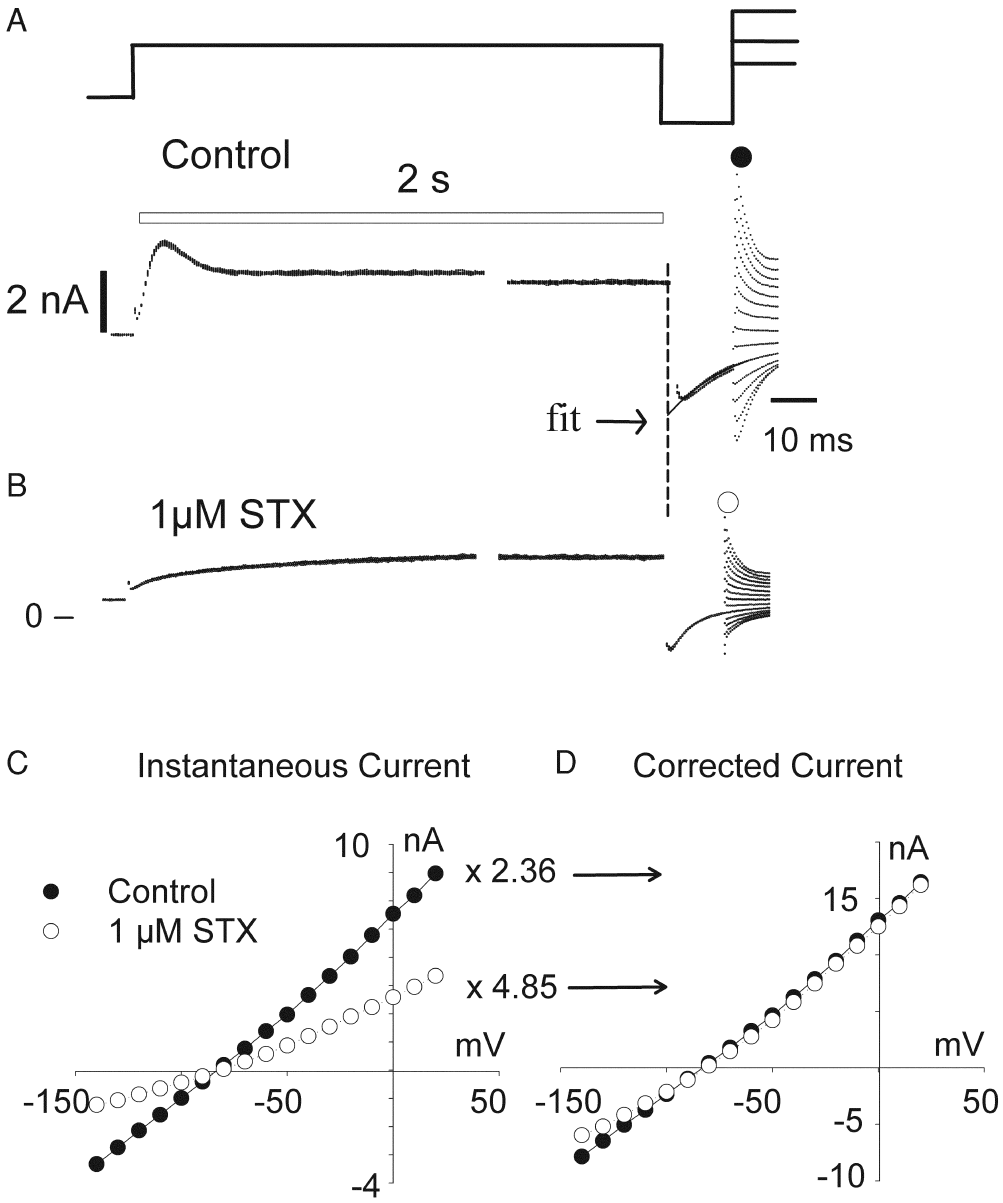

FIGURE 3. Effects of STX on open hERG K^+ channels. K^+ currents through open The hERG channels were estimated as shown in A (control) and B (1 μM STX). The cells were held at −80 mV. A 2-s step to 50 mV was used to activate hERG K^+ channels, followed by a 12.5-ms step to −100 mV to recover channels from the inactivated to the open state, then step potentials between 100 and −140 mV were applied to record K^+ current through open hERG channels. Note the change in time scale. On the right side of A and B, current traces after the 2-s condition pulse are shown at the expanded time scale. The amount of hERG K^+ current deactivation during 12.5 ms at −100 mV was extrapolated to the time of the voltage transition to correct for deactivation before the test step. The kinetic correction factor described in Johnson et al. (1999a) was used to correct for the underestimate of the peak current due to deactivation during the 12.5-ms recovery period. The I-V relationship of instantaneous hERG K^+ current before correction is shown in C. The I-V relationship corrected for hERG K^+ current is shown in D. $[Ca^{2+}]_o$ = 0.1 mM, 36°C.

as those illustrated in Fig. 3 to probe the effects of STX on K^+ current through the open channel. Here channels were driven into open and inactivated states during the step to 50 mV. Repolarization to −100 mV for 12.5 ms allows channels to exit the inactivated state into the open state from which they more slowly deactivate. The subsequent step to various potentials reveals the fraction of channels that were open. Using this method there was an apparent decrease in the current measured immediately upon stepping to open the channels. Note that I-V curves remained essentially linear in STX. If we account for the change in kinetics during the step to −100 mV, the decrease was caused solely by the change in kinetics and not by direct pore block (Johnson et al., 1999a). This distinguishes STX from other agents and ions that appear to interact with P-domains (Mitcheson et al., 2000; Numaguchi et al., 2000a,b; Mullins et al., 2002; Pardo-Lopez et al., 2002).

The effects of STX were further evaluated using a voltage-ramp analysis on hERG K^+ channels. Membrane potential was changed continuously (ramped) across the channel voltage activation range. Fig. 4 shows examples of this analysis, comparing a known pore blocker, MK499 (Mitcheson et al., 2000), and STX. STX shifted the ramp window current confirming the shift in activation threshold and the limited effect at strongly positive membrane potentials. The maximum suppression seen in STX (Fig. 4, middle and bottom) occurred near the midpoint of the voltage activation curve due to the shift of this relationship. In contrast, 10 nM MK499 caused the maximum reduction when most channels were open (near 0 mV). Inhibi-

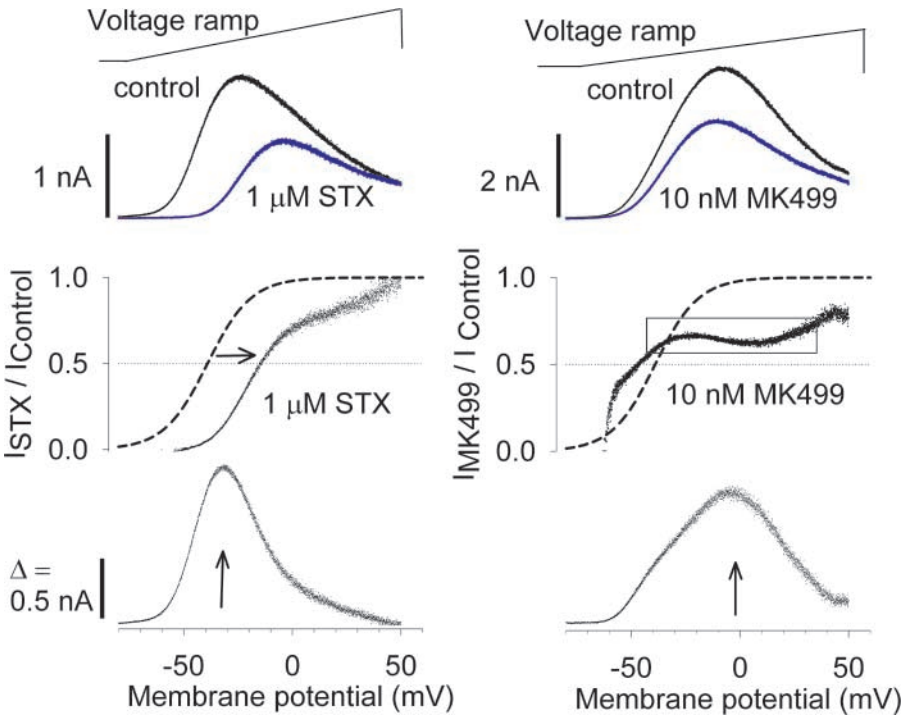

FIGURE 4. Voltage ramp analysis of the effects of STX on hERG K^+ channels. Membrane potential was ramped across the voltage activation range of the channels. The left panels show the effects of STX. The right panel shows the effects of MK499, a hERG pore blocker. (Top) K^+ currents recorded during a ramp protocol in control or drug (concentrations shown). (Middle) Ratio of ramp current in drug to control ($I_{drug}/I_{control}$). The best fit Boltzmann estimated from tail currents is shown also for reference. (Bottom) Drug-sensitive K^+ current estimated by subtracting the K^+ current recorded in drug from the K^+ current in the absence of drug.

tion was less when fewer channels were open (−60 to −40 mV), and was relatively constant between −40 and 40 mV (fractional current was ~0.6). Experiments coadministering STX (1–3 μM) and MK-499 (10 nM; unpublished data) indicated that the effects of these two agents were additive, suggesting unique sites of action and distinct mechanisms. In other experiments (unpublished data) STX (10 μM) was included in the intracellular pipette solution with no effect, suggesting an extracellular site of action.

STX Modulates hERG K^+ Channel Gating

To explore the mechanism of the STX–channel interactions both kinetically and in steady-state in more detail, we employed a rapid drug delivery device similar to that used for ligand-gated channels. This approach permits rapid assessment of association and dissociation of STX. Fig. 5 shows the use of this method. Calibration studies showed this method could effect a solution change measured as alterations in electrode junction potential with time constants <10 ms (unpublished data). To establish the actual times in the whole-cell recording mode, we used several probe agents, including 40 mM KCl and ergtoxin (ErgTx). ErgTx is a ERG-specific scorpion peptide toxin that recognizes the P-region of hERG channels, and blocks the pore with an apparent K_D of 12 nM (Gurrola et al., 1999; Scaloni et al., 2000; Pardo-Lopez et al., 2002).

Fig. 5 A shows rapid application of bath solution (control), stepping the same solution from two different pipettes on and off the cell during a prolonged depolarization to −30 mV. Fig. 5 B shows application of 40 mM KCl (positive control) followed by a bath test solution. The change in external K^+ altered the driving force for the K^+ current through open hERG channels. The change in K^+ current occurs as rapidly as the channels are exposed to the new K^+ concentration. The change of K^+ current upon return to the control K^+ concentration was equally rapid. In Fig. 5 C, control solutions are switched. Fig. 5 D shows the lack of effect of 1 mM acetic acid and 10 μM tetrodotoxin (TTX). Acetic acid is present in the stock solutions of TTX and STX. Upon application of ErgTx (20 nM, Fig. 5 E), the current decreased rapidly and recovered upon changing to the control bath solution. Whereas the KCl induced change in driving force reversed rapidly as expected (Fig. 5 B), the method shows the expected slow off-rate of ErgTx.

When 3 μM STX was rapidly applied to a cell clamped at −30 mV (Fig. 5 F) the hERG K^+ current first increased and then declined. This was a surprising and unexpected observation. The fact that this was not seen with either changes in $[K]_o$ or ErgTx or solution changes indicated that this was not an artifact of the method. These experiments show the specificity and rapidity of the rapid solution change and that the increase and decreases seen in STX are attributes of the compound and not an artifact of the method.

What can be a mechanism for the paradoxical dual effect of STX? We first characterized the concentration dependence and kinetics of these process(es). Fig. 6 shows the application and washout of increasing con-

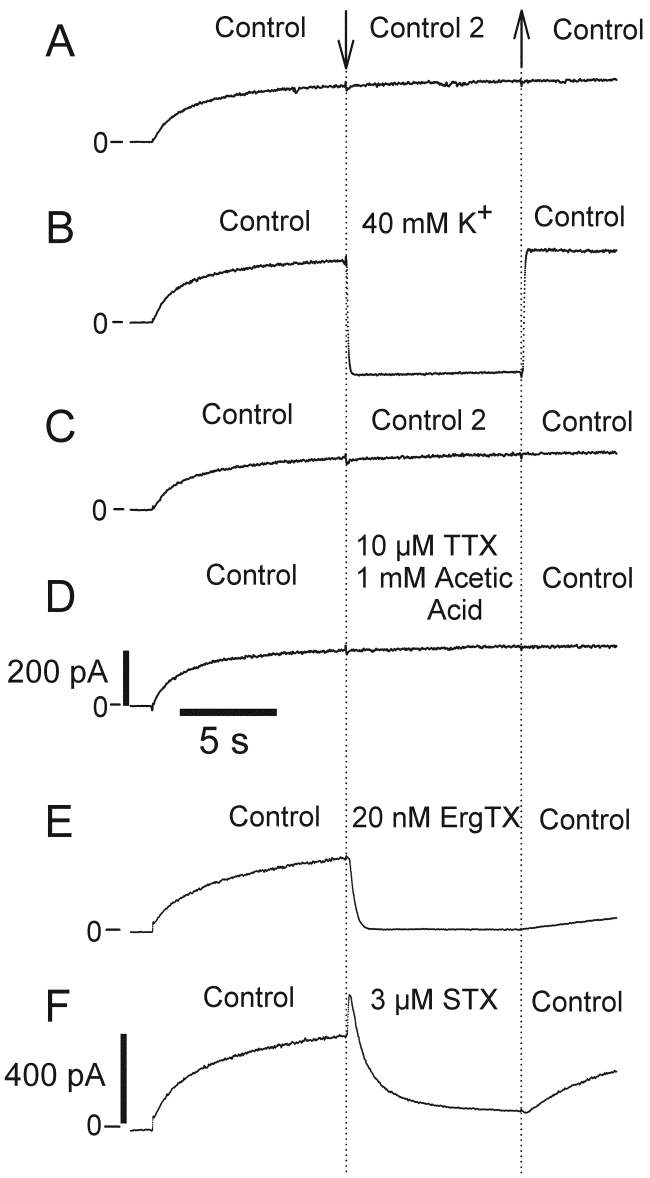

FIGURE 5. Controls for rapid solutions changes: effects on hERG K^+ channels. Test solutions were delivered to the channels by a rapid solution exchange device. Cells were clamped at −80 mV and stepped to a membrane potential of −30 mV for 25 s. During this voltage step, a programed fast step perfusion device was used to apply various agents at t = 10 s and a wash solution at t = 20 s. Shown are the following solution changes (A) bath solution (control); (B) 40 mM KCl; (C) bath solution (wash, same as 1); (D) 10 μM TTX + 1 mM acetic acid (STX excipiant); (E) 20 nM rErgtoxin; (F) 3 μM STX. Similar results were obtained on a total of four cells. $[Ca^{2+}]_o$ = 0.1 mM, 23°C.

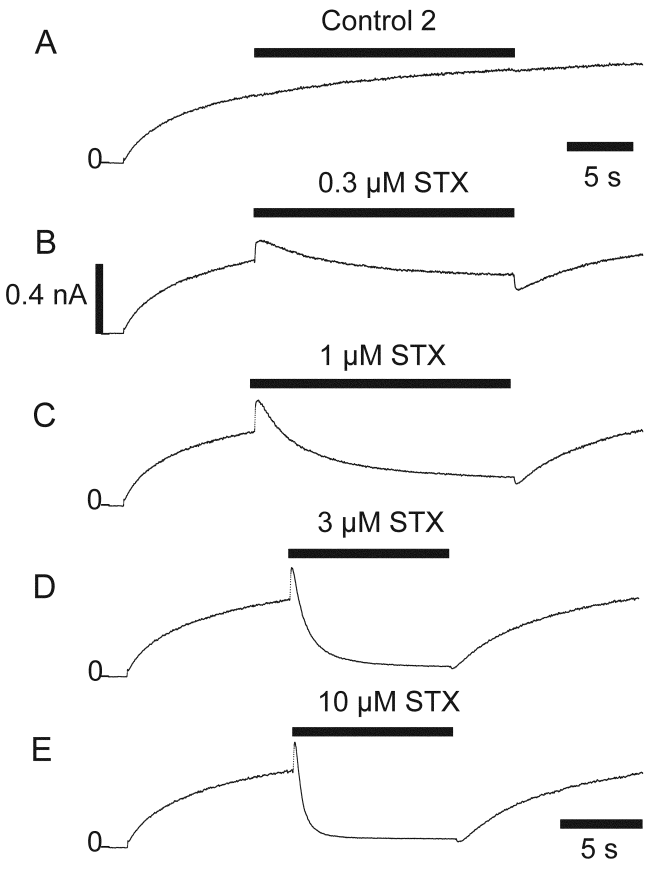

FIGURE 6. Rapid application of STX: kinetic analysis and concentration dependence of increase and decrease of hERG channel K^+ currents. STX was delivered to the cells by a fast-step dual channel perfusion device. Cells were voltage clamped to −80 mV and stepped to −40 mV for 38 s in control (A), 0.3 (B), and 1 μM STX (C) or 25 s for 3 (D), and 10 μM STX (E). During this voltage step, a rapid solution exchange occurred at 10 s indicated by the bar above each record. A wash solution started at 30 s (control, 0.3, 1 μM STX) or at 20 s (3 and 10 μM STX). $[Ca^{2+}]o$ = 0.1 mM, 23°C.

centrations of STX during a prolonged depolarization. Both the magnitude and the rate of the response changed with STX concentrations. The K^+ current through open hERG channels first increased and then declined. Upon switching back to the control solutions (wash) the K^+ current returned to the control level. Fig. 7 summarizes the change in magnitudes of the rising and declining components of K^+ current caused by different concentrations of STX. STX caused nearly a 40% increase in K^+ current through open hERG channels followed by a large decrease. The EC_{50}s obtained by fitting these data with the Eq. 4 were 0.27 and 0.47 μM, respectively.

The rising and declining phases were fit separately to characterize their main kinetic features. Although this approach was arbitrary and should not be interpreted to imply a mechanism, it is a convenient method for quantitation of the time courses. The results are shown in Tables III and IV. The rising phase was analyzed by fitting an exponential function to estimate the time constants. The best fit was determined by nonlinear least squares regression and by visual inspection of the residual differences between the data and the fitted equation. Figs. 5 and 8 illustrate how the initiation of

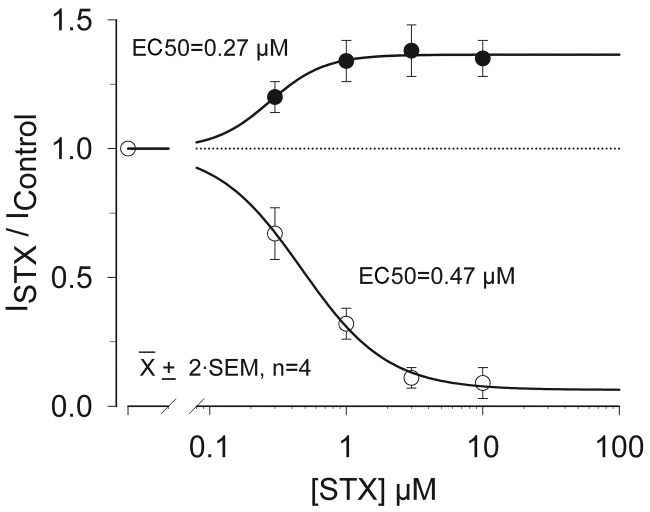

FIGURE 7. Summary of concentration dependence of increases and decrease of K^+ currents. The fractional increase and decrease of K^+ current at each concentration of STX is plotted as a function of STX concentration and was fitted with Eq. 4. The solid curves represent best fits of Eq. 4 with apparent EC_{50}s were 0.27 and 0.47 μM, respectively.

the solution change was determined. An electrical artifact is apparent in the current recording when the perfusion pipette change first occurs. The data from the rate of change caused by extracellular 40 mM KCl were used to define the limit of exchange rates (Fig. 5 B).

The declining phase of the current during application of STX was measured and quantitated by fitting the time course with an exponential function to obtain the STX-dependent time constants. This analysis ignored (excluded) the rising phase caused by STX if present. STX caused a concentration-dependent increase in the rate of current decay. The best fitting equation consisted of 2 exponential components (2 time constants). As the concentration of STX was increased, the proportion of the faster process increased from 0.08 at 0.3 μM to 0.83 at 10 μM (Table III).

Fig. 8 shows the effect of rapid application of 3 μM STX at two different membrane potentials: 30 and −30 mV and unique kinetic changes observed. During a step to 30 mV, application of STX rapidly increased the K^+ current. The rates and magnitude of the increase in K^+ current caused by 3 μM STX were the same at −30 and 30 mV (Fig. 8 C). This indicates that the STX effect was established very rapidly. In contrast to the subsequent decrease in K^+ current caused by STX at −30 mV, the current remained elevated during the 10-s exposure at 30 mV. Upon return to the bath solution (STX washout), the rates of recovery were very different at −30 and 30 mV, respectively. At 30 mV, the K^+ current returned to control levels upon washout with a time constant of 120 ms (τ = 0.12 s). The recovery upon washout of STX was much slower at −30 mV and occurred after a delay (τ = 1.2 s, τ = 8 s). The time course of recovery to control levels required >10 s at −30 mV (Fig. 8 E). This suggested that the rates of change of K^+ current caused by STX may reflect in part the intrinsic rates of gating of the channel, and not simply the rates of association and dissociation of STX. The time constants for activation of hERG channels at −40 mV in the absence of STX were 2.6 ± 3.3 and 25.6 ± 5.3 s (n = 8). These time constants contributed equally (A_F = 0.49 ± 0.04). The lack of a simple first order dissociation process and the membrane potential effects were intriguing, and further suggested a complex binding scheme or mechanism of channel modification. Possibilities include changes in binding affinity or access to the binding pocket dependent upon membrane potential, or modified gating.

Concentration-dependence of STX-induced Decrease in K^+ Current

If the rise and decline of K^+ currents are caused by STX association with the channel, there should be a discernible concentration dependence. A first order interaction driven by mass action should show an increase in the response rate with increased concentrations. When plotted against concentration, the rate should increase as a linear function of concentration with a slope equal to the on rate constant and the zero concentration y-intercept equal to the dissociation rate constant. Examination of the data analyzed in this manner clearly indicated that a simple 1st order binding interaction but did not fit the data. The concentration dependences of rates of change of K^+ currents caused by STX are summarized in Fig. 9 A. The time course of STX-induced change in K^+ current at −40 mV required a two-exponential function to estimate the rate of change and the fractional amplitude. The rates of

TABLE III

STX Concentration Dependence Time Constants of Decrease in hERG Current at −40 mV at 23°C

STX (μM)	0.3	1	3	10
τ_F (s)	1.7 ± 0.2 (3)	1.5 ± 0.1 (9)	0.68 ± 0.03 (20)	0.40 ± 0.03 (11)
τ_S (s)	6.5 ± 0.4 (11)	6.0 ± 0.5 (12)	2.8 ± 0.3 (20)	1.9 ± 0.2 (10)
$A_F/(A_F+A_S)$	0.08 ± 0.04 (11)	0.36 ± 0.07 (12)	0.69 ± 0.02 (20)	0.83 ± 0.02 (11)

Mean ± SEM (number of cells).

TABLE IV

The Voltage Dependence of 3 μM STX hERG Current Kinetics 23°C

	−50 mV	−40 mV	−30 mV	−20 mV	−10 mV
τ_F (s)	0.5 ± 0.08 (5)	0.57 ± 0.09 (4)	0.6 ± 0.04(9)	0.65 ± 0.06(4)	0.85 ± 0.11(4)
τ_S (s)	2.4 ± 0.5 (5)	2.3 ± 0.4 (4)	2.7 ± 0.3 (9)	3.4 ± 0.2 (4)	5.1 ± 1.2 (4)
$A_F/(A_F+A_S)$	0.73 ± 0.05 (5)	0.61 ± 0.03 (4)	0.57 ± 0.02 (9)	0.43 ± 0.01 (4)	0.44 ± 0.02 (4)
	0 mV	10 mV	20 mV	30 mV	40 mV
τ_F (s)	0.94 ± 0.18 (3)				
τ_S (s)	4.5 ± 0.8 (4)	3.3 ± 0.2 (4)	5.8 ± 1.5 (3)	3.4 ± 0.1 (2)	5.7 (1)
$A_F/(A_F+A_S)$	0.30 ± 0.10 (4)	0 (4)	0 (3)	0 (2)	0 (1)

Mean ± SEM (number of cells).

change in current (reciprocal of the fitted time constants: $1/\tau$) were derived from the two time constants of the exponential fits (τ_F and τ_S). The rates of activation gating in the absence of STX at −40 mV are plotted as a reference. The gating process had reached steady-state before STX application in these experiments. It appeared as if STX affected channel gating as the observed STX-induced rate increases from the control gating rates in the absence of STX. The concentration—rate plot was nonlinear. The fractional amplitude (A_F) of the faster component associated with τ_F is plotted in Fig. 9 B and increased with [STX]. These results demonstrate that there was a concentration-dependent increase in the rate and magnitude of the effect (decrease in K^+ current), and suggest a rather complex concentration-depen-

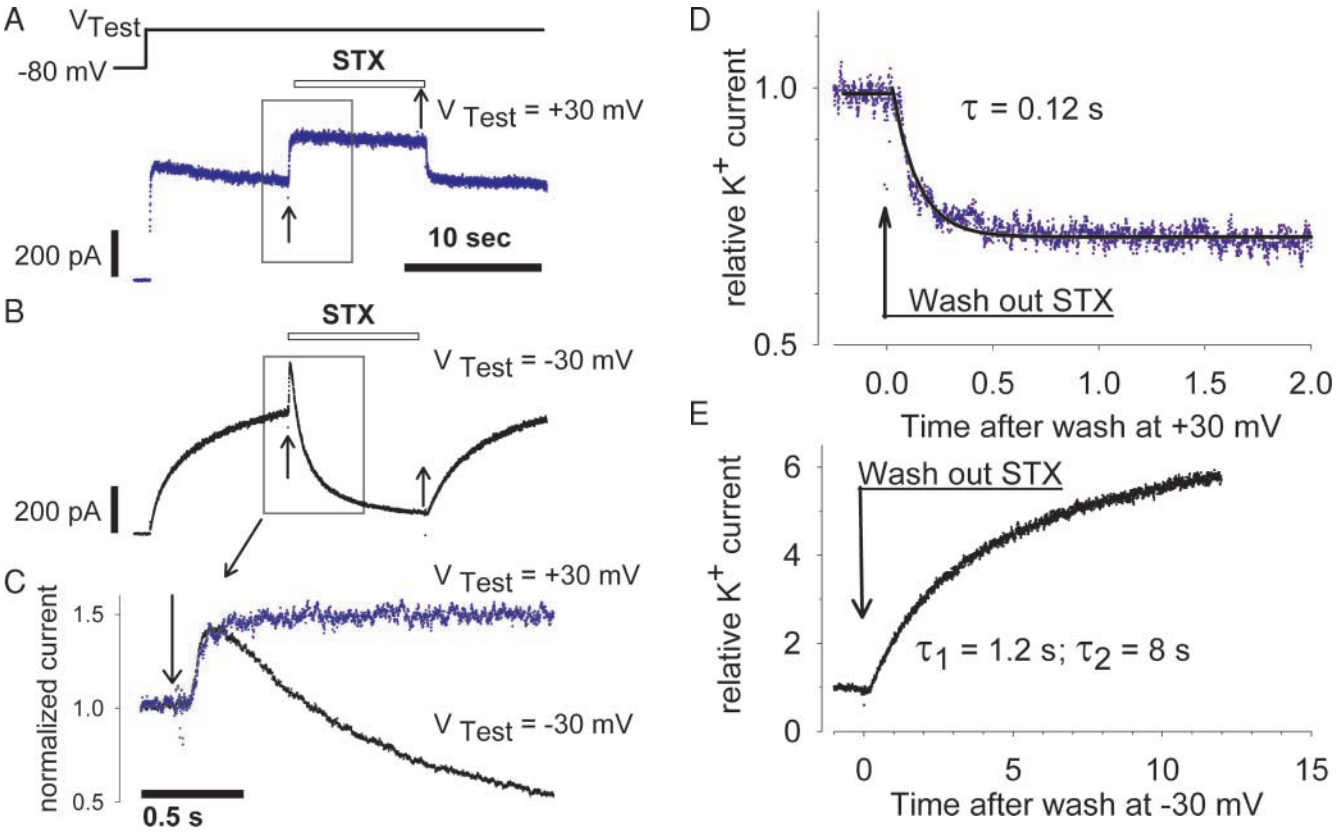

FIGURE 8. Dual effect of STX on K^+ current depending upon membrane potential. The cell was held at −80 mV and stepped alternatively to −30 or 30 mV for 30 s. During this long depolarization after 10 s, STX was applied for 10 s and washed out. (A) Membrane potential step to 30 mV; (B) membrane potential step to −30 mV; (C) superposition of K^+ currents at each voltage step. The current data in the gray boxed areas in A and B were scaled to be 1 immediately before STX application. (D) Wash out of STX at 30 mV. (E) Wash out of STX at −30 mV. In D and E, the time axis was translated so that the beginning of the washout corresponded with t = 0. The solution switch electrical artifact can be seen as noise on the current trace. The application and removal of STX is also indicated by the arrows.

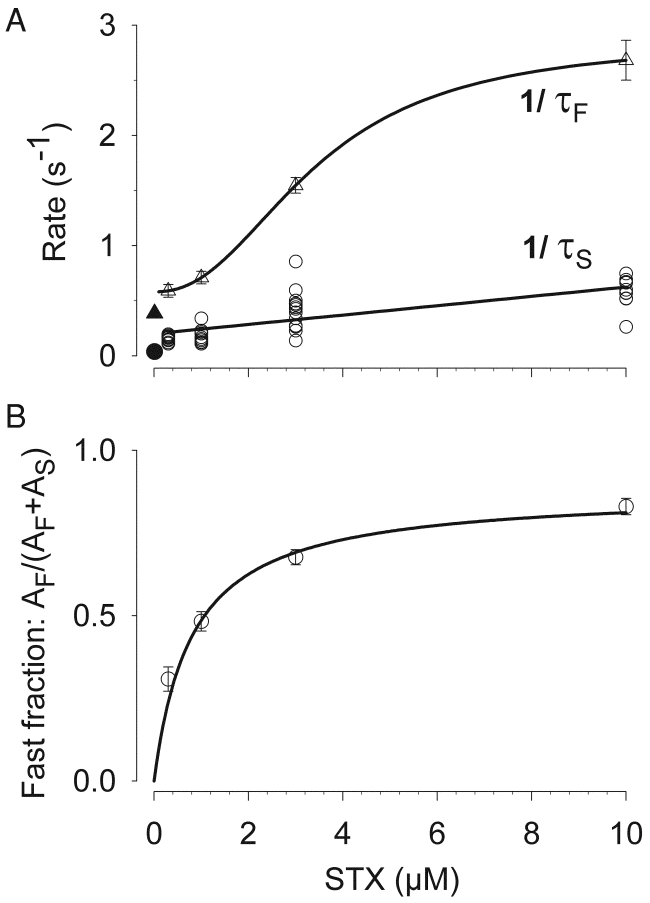

FIGURE 9. (A) Concentration dependence of rates of change caused by STX. The time course of STX-induced K^+ current decrease at −40 mV was fitted to a two-exponential function to estimate the rate of change and the fractional amplitude. The rates of change in current ($1/\tau$) were derived from the two time constants of the exponential fits (τ_F and τ_S). (B) The fractional amplitude (A_F) of the faster component associated with τ_F is plotted as a function of STX concentration. The control rates of gating in the absence of STX are plotted as solid symbols for reference.

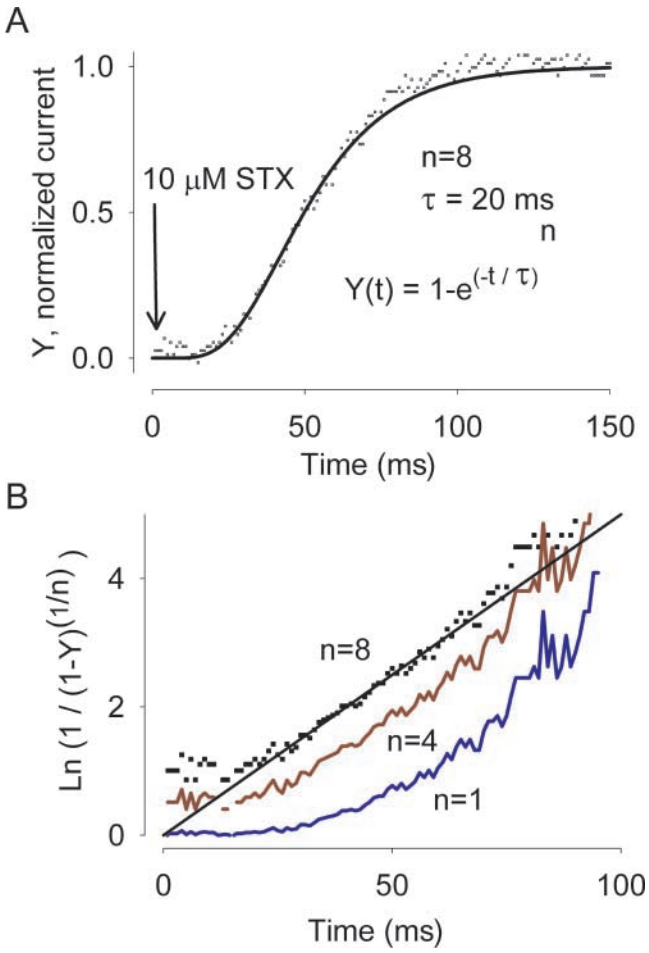

FIGURE 10. Analysis of the increase of hERG K^+ currents after rapid application of 10 μM STX during a long (30 s) voltage clamp step to −40 mV. Justification for STX-channel stoichiometry ≥4. Data were scaled to a maximum of 1 at steady-state and fit with an exponential function compatible with n independent binding sites. $Y(t) = (1 - e^{(-t/\tau)})^n$. Alternatively, the normalized data (Y(t)) were transformed with various roots of the equation, $\ln(1/(1 - Y)^{1/n}$ and plotted as a function of time B. After this transformation, the data should be linearized when the root ($1/n$) matches the appropriate number of sites. Transformations with $n = 1$ or $n = 4$ resulted in nonlinear datasets, if $n = 8$, then the data were linearized.

dent interaction between STX, its binding site(s), and channel gating.

Cooperativity and Kinetics of Channel Modification

We were interested in exploring in more detail the interaction between STX and the channel. We examined the kinetics of the STX induced rising phase of the K^+ current in greater detail as shown in Fig. 10. In panel A, the first 150 ms after rapid application of 10 μM STX are shown. The increase in current began after a time lag. To estimate the kinetics of this process, the data were transformed as shown on the ordinate of Fig. 10 B $\ln[1/(1 - Y)^{1/n}]$. Here Y is the fractional current shown in Fig. 10 A. Fig. 10 B shows this operation on the data with n equal to 1, 4, and 8. Note that the eighth root of the data leads to the log-linear plot. The solid curve in Fig. 10 A was calculated from the equation

$$Y(t) = (1 - e^{-t/\tau})^n, \quad (5)$$

where $n = 8$. The curve is expected if there are n independent sites whose occupancy is necessary and sufficient for the full effect. Attempts to fit these with smaller values of n could not describe the data adequately. Note that small errors in the time in which STX concentrations reached steady-state will affect the lag seen. We caution against placing too much emphasis on the exact magnitude of the number of sites, but

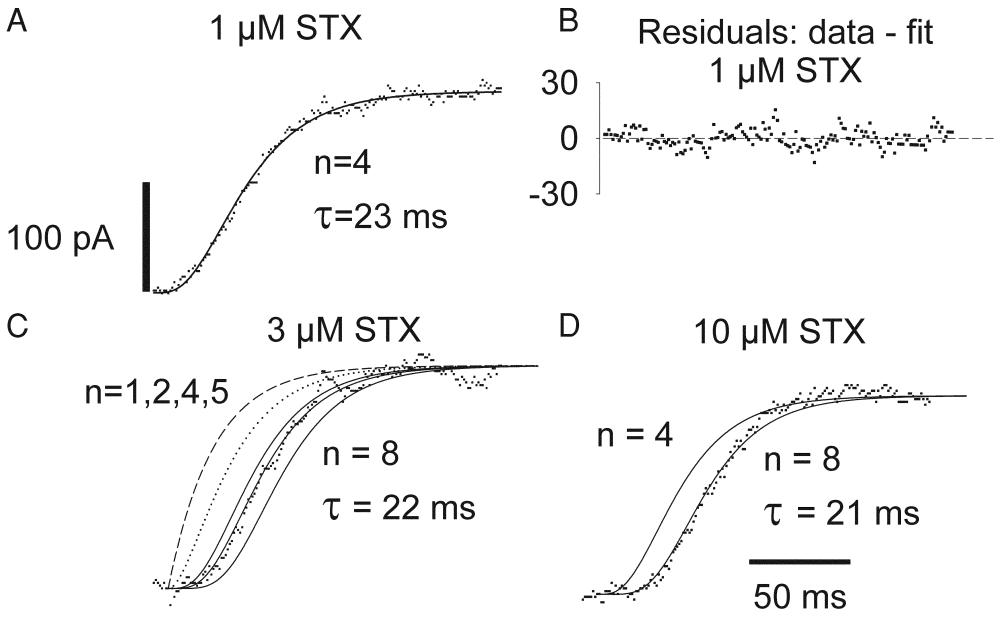

FIGURE 11. Analysis of the increase of hERG K^+ currents following rapid application of STX. (A) Rapid application of 1 μM STX. The best fit of a higher order exponential function [$y(t) = A \cdot (1 - e^{(-t/\tau)})^n + C$] is shown superimposed. The best fit power (n) was 4. The residual error between the fit and the data is shown in B. C and D show the increase of hERG K^+ currents following rapid application of 3 and 10 μM STX, respectively. Also shown are evaluation of the above equation with different values of the parameter, n. In C (3 μM STX), a value of $n > 4$ fit the data. In D at a higher concentration of STX (10 μM), $n = 8$ appeared to fit to the data. $[Ca^{2+}]_o$ = 0.1 mM, 23°C.

the data seem to clearly indicate that multiple sites are involved.

We explored this further with additional concentrations of STX as shown in Fig. 11. Here the same type of normalized STX-induced K^+ current data are shown. In Fig. 11 A, the effects of 1 μM STX are shown with the best fit of Eq. 5. In this case $n = 4$. The residual differences between the fit and the data are shown in Fig. 11 B. It can be seen that the fit is very good and the residuals are randomly distributed ($F < 0.05$). Attempts to force fit these data with other values of n were unsuccessful, and manual generation of curves from Eq. 5 with different values of n is informative. Fig. 11 C shows normalized STX-induced K^+ current data for 3 μM STX. Also shown are curves generated from Eq. 5 with $n = 1, 2, 4, 5, 8$. It can be seen that the data (dots) fall between curves with n values of 4 and 5. In Fig. 11 D a similar analysis is shown for 10 μM STX. Here again $n > 4$ was required. We do not think the these experiments can precisely define the stoichiometry of the STX-hERG interaction, but these experiments and analyses show without question that more than one STX molecule interacts with each hERG channel protein and it is likely that the STX-hERG stoichiometry is at least four or more STX per channel.

STX Behaves Like a Negative Membrane Potential Step

Are the dual effect of STX seen at some membrane potentials and the opposite effects seen at others consistent with a gating modifier agent? Can we explain this apparently paradoxical behavior in terms of a self-consistent change in some aspect of channel gating? To explore the hypothesis that STX directly modified voltage sensing and biased channel gating much like a small change in membrane potential, we used small voltage jumps to probe the kinetic changes seen when applied in a manner analogous to rapid application of STX. If STX modifies the voltage dependence of activation and inactivation, a small change in membrane potential riding on top of a voltage step should mimic STX depending on the relative positions of the voltage activation and inactivation curves and the membrane potential step. If STX shifts these curves to the right (shifts in P_{open}), then a small negative step (10 mV) in control should mimic this by moving the system to a new P_{open} (gating) value. A negative step will decrease K^+ current at potentials where the voltage-activation process dominates, but at potentials where inactivation is dominant, a small hyperpolarization should relieve inactivation and increase the current. We tested these ideas in a series of experiments exemplified in Fig. 12. K^+ current was converted to conductance to account for the changes in K^+ current caused solely by changes in driving force for K^+. The analysis of conductance focuses on the changes in gating. Under the limited conditions tested, these small perturbations partially mimicked the effects seen with STX. At negative potentials a decrease in conductance was seen, and at more positive potentials where activation nears saturation and inactivation dominates, a small negative test actually increased the macroscopic conductance ($\gamma \cdot N \cdot P_{open}$). At more extreme depolarizations where both processes are near saturation, the effect diminished. Recognizing that a 10-mV step will not perfectly reproduced the STX ef-

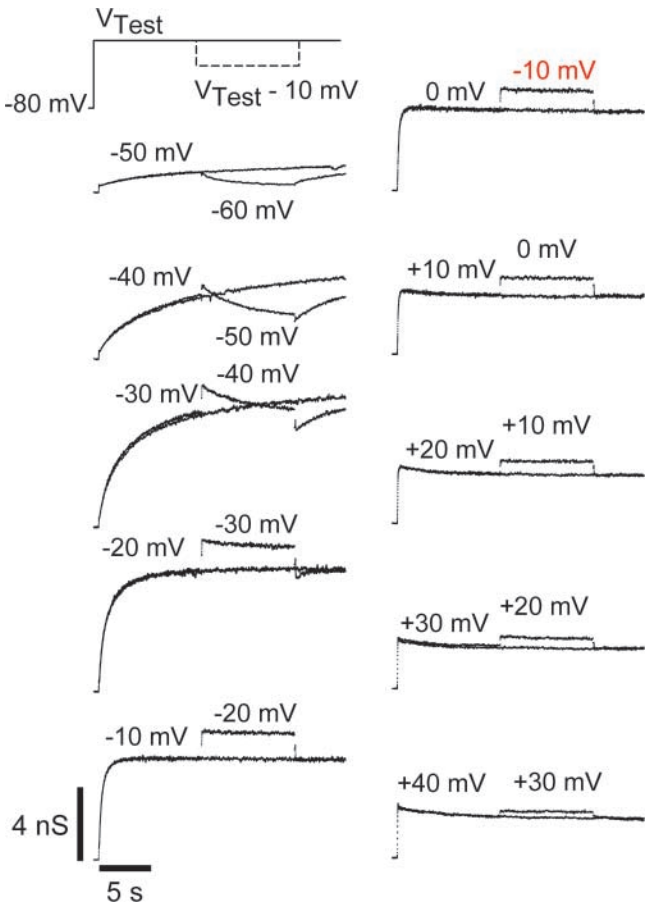

FIGURE 12. A 10 mV negative voltage step mimicked STX effect on hERG K^+ currents. No STX was used in this experiment. This voltage clamp protocol consists of two episodes. The first episode was a 25-s test pulse (V_{1st}) that changed from −50 to 40 mV in 10-mV increments. During the second episode, the 25-s duration was divided into three parts: 10, 10, and 5 s. The first 10 s and the last 5 s were set to the same membrane potential voltage as V_{1st}. During the middle 10 s the membrane potential was stepped negative by 10 mV relative to V_{1st}. hERG K^+ currents were converted to chord conductances by dividing the amplitude of the current with its corresponding driving force (Vm- Vrev). The reversal potential (Vrev) used for hERG K^+ channels was −92 mV. $[Ca^{2+}]_o$ = 0.1 mM, 23°C.

fect if there is a differential effect on the two relationships, the results are quite compelling.

We explored this hypothesis further using a computational approach. We used the model presented in Johnson et al. (1999a) and incorporated the ability to add a bias voltage into the rate constant master equations. This permitted a kinetic evaluation of a "voltage shift" as might be caused by STX affecting the voltage sensor(s). Surprisingly, the effects of STX are predicted by this simple model. The results are shown in Fig. 13. The voltage activation and inactivation curves are shown along with the shift that produced the effects seen. The kinetic "experiment" was designed to mimic the STX addition. The "voltage-clamp protocol" shows the temporal order of the "experiment." In this model the kinetics are solely determine by the voltage-dependent rate constant equations (Fig. 13, legend). During a voltage clamp step, a small voltage bias was added to the voltage-dependent term of the rate constant equation at 3 s. After another 3 s this bias was removed. If STX modifies voltage sensing, this should mimic its action. The resulting P_{open} time courses are shown. Each represents a simulation at a different applied membrane potential. A different bias potential (ΔVa and ΔVi) was applied to the rate equations that govern "activation" (α, β) compared with inactivation (κ, λ). But in all cases the magnitude was the same: ΔVa was 30 mV and ΔVi was 10 mV. The model predicts a jump in P_{open} when a step to 30 mV is applied and a decrease in P_{open} when a step to a negative potential (e.g., −50 mV) is applied. At membrane potentials in between, there was a transient increase followed by a decrease in P_{open}. The steady-state gating parameters and the fractional open probability are also shown. The top panel shows the availability curves (not inactivated) and the voltage activation curve (voltage dependence of channel opening with inactivation removed). The bottom panel shows the steady-state "window current" generated by the overlap of these relationships and is analogous to the data seen in Fig. 1 and illustrates the mechanism for limited effect observed in the ramp analysis at potentials positive to 0 mV. The magnitude of the applied shift is seen and the effect on the steady-state P_{open} translates into an effect on K^+ current.

DISCUSSION

We have shown that STX shifted the voltage-activation process to more depolarized membrane potentials, stabilizing the closed channel, slowed activation-gating kinetics during depolarization, and accelerated deactivation-gating kinetics at negative membrane potentials. During rapid application, STX increased the K^+ current at some membrane potentials, decreased it at others, and at intermediate membrane potentials cause both an increase followed by a decrease. Although the changes in the channel were readily reversible, the dissociation kinetics were dependent on concentration and membrane potential, a property not consistent with a simple first order binding and dissociation process. The results suggest STX modifies channel gating in a complex manner and that there are likely multiple cooperatively linked binding sites. Further the results are consistent with an STX-induced shift in the voltage dependence of the rate constants that govern channel opening and inactivation. Although we interpret these findings specifically within the context of ion channel gating, the results are very general and consistent with the theory of allosteric modulation of proteins (Monod et al., 1965; Changeux and Edelstein, 1998).

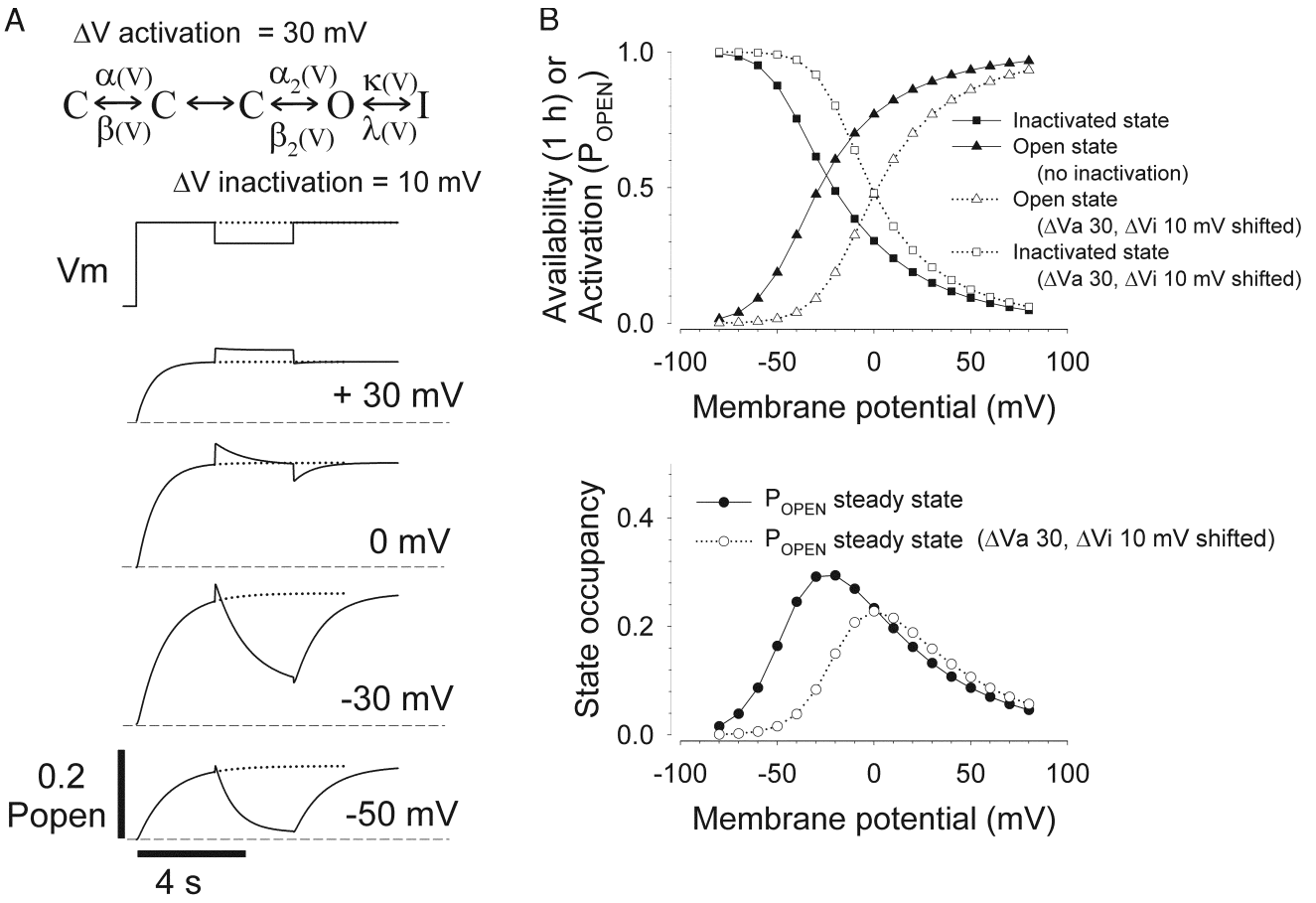

FIGURE 13. A simple K^+ channel kinetic model predicts STX effects through shifting activation and inactivation gating. Simulation of STX action through modification of voltage-dependent rate constants. The model employed was that of Johnson et al. (1999a) as modified from Wang et al. (1997). The effects of STX were simulated by perturbing the voltage-dependent rate constants governing activation (α and β) and inactivation (κ and λ). A 30 mV (α and β) and a 10 mV (κ and λ) shift (ΔV) was added to the voltage-dependent term of the rate constant master equations to mimic the effect of STX. The top panel shows the voltage clamp protocol and the perturbation (ΔV) to the rate equations is indicated as a small step. As indicated schematically in the top of A, the rate constant equations were temporarily modified for 3 s during the voltage step, beginning 3 s after the step initiation. The applied voltage and hence driving force were not actually changed. The dotted lines in the P_{open} traces indicate the control behavior in the absence of the shift. The model is shown schematically where α, β, κ, and λ are voltage-dependent rate constants defined by the following equations. Closed, open, and inactivated (closed also) states are symbolized as C, O, and I, respectively. $\alpha = \alpha_o \exp^{[z\delta e (V + \Delta Va) / k_B / T]}$ forward; $\beta = \beta_o \exp^{[z(1-\delta) e (V + \Delta Va)/k_B/T]}$ reverse; $\kappa = \kappa_o \exp^{[z\delta e (V + \Delta Vi)/k_B/T]}$ forward; $\lambda = \lambda_o \exp^{[z(1-\delta) e (V + \Delta Vi) / k_B / T]}$ reverse. α is the forward rate constant (s^{-1}); α_o is value of α in the absence of an electric field. zδ the gating charge and the fraction of the field it senses, e the electron charge, k_B is Boltzmann's constant, T is the absolute temperature, V is membrane potential, and ΔV is a bias potential that can be applied to the equations. The effect is to shift the log linear rate constant relationship along the voltage axis.

The Mechanism of STX Modulation

The two main changes in hERG K^+ current caused by STX (Fig. 1 and 2) observed at steady-state were the reduction of current amplitude and the shifting of activation curves toward more positive membrane potentials. STX, acting as a hERG K^+ channel–gating modulator, alters membrane potential dependence of the open probability.

We can rule out a simple pore block mechanism based on several experimental observations. The decrease in current was greatest at membrane potentials where the activation curve was shifted the most, not where P_{open} was maximal (as expected for a open state pore blocker). There was no tail current crossover as is seen with some open state blockers that slowly dissociate from the open state during channel closure. The effects of STX were quite distinct from known pore blockers: MK-499 and ErgTx. Fig. 3 shows that STX failed to affect instantaneous hERG K^+ current except through changes in gating. STX seemed to stabilize the closed state of hERG channels.

STX and TTX are nonpeptide toxins shown to bind to the outer pore of the sodium channel such that they inhibit Na^+ flux (Kao and Nishiyama, 1965; Kao 1966; Narahashi et al., 1967; Chiba and Hashimoto 1969;

Evans, 1969; Wong et al., 1971; Kao, 1972; Narahashi 1972; Henderson et al., 1973; Campbell and Hille, 1976; Wagner and Ulbricht, 1976; Noda et al., 1989; Lipkind and Fozzard, 1994; Satin et al., 1994; Penzotti et al., 1998). Although the chemical structure of TTX is very different from that of STX, the fact that these toxins have the same sodium-channel binding-site suggests that their three dimensional (3-D) structures have some similarities that allow them to dock into the sodium-channel pore effectively (Penzotti et al., 1998). These similarities, however, did not translate to hERG K^+ channels because TTX, unlike STX, had no effect. TTX carries a single positive charge, while STX has two. It is plausible that two positive charges of STX play a role in modifying hERG K^+ channel gating. Divalent cations, such as Ca^{2+}, Mg^{2+}, and Cd^{2+} influence hERG K^+ channel gating (Ho et al., 1998; Johnson et al., 1999a,b, 2001; Po et al., 1999; Sanchez-Chapula and Sanguinetti, 2000). In particular, the effects of Ca^{2+} on hERG K^+ channels are similar in some respects to STX (Johnson et al., 1999a), but less potent. Ca^{2+} shifts channel voltage activation to more depolarized potentials, slows activation gating kinetics, and accelerates deactivation gating kinetics (Johnson et al., 1999a).

We can compare STX with other gating modifiers. The behavior of STX-modulating hERG K^+ channels is in some regards similar to hanatoxin (a Kv2.1 K^+ channel gating modifier) and ω-Aga-IVA toxin (a calcium channel gating modifier). These toxins reduce current amplitude and shift voltage activation gating to more depolarized membrane potentials (Swartz and MacKinnon, 1997a,b; Li-Smerin and Swartz, 2000).

Experiments using intracellular STX showed no effect on the channel (unpublished data), suggesting that STX acts externally. If the STX-binding sites are located near the voltage-sensor (S4) domains of hERG K^+ channels, effects on gating through charge–charge or charge–dipole interactions may be expected. These S2-S3-S4 domains are implicated in the binding for divalent cations and for channel-gating modifiers (Swartz and MacKinnon, 1997b; Winterfield and Swartz, 2000; Silverman et al., 2000). Silverman et al. (2000) showed that the EAG channel with a point-mutation of S2 at D278V or S3 at D327A did not respond to changes in external Mg^{2+} concentration, while external Mg^{2+} significantly slowed the activation process of the wild-type EAG channel. These two amino acids (D278 and D327) are conserved in the hERG K^+ channel (Silverman et al., 2000), implicating this region as a candidate. A link between the STX binding site and the voltage-sensing domains is suggested by our experimental results. A 10-mV step alone was able to partially mimic the effects of STX (Fig. 12). The steady-state and kinetic effects of STX are predicted by a simple K^+ channel model in which the voltage-activation and inactivation relationships are shifted to depolarized potentials (Fig. 13).

The Stoichiometry of the STX-hERG K^+ Channel Interaction

Voltage-gated K^+ channels are believed to be composed of four α subunits, each possessing six transmembrane segments (S1–S6). The first four segments (S1–S4) of one α subunit form a voltage-sensing module, and the four equivalent voltage-sensing domains surround the central pore domain (S5-P-S6) to form an ion channel (Li-Smerin et al., 2000). This fourfold symmetry around a central pore places constraints upon binding site topologies. Hence, if binding involves the voltage-sensing domains (including the S4 domains), each channel has at least four potential sites. (Swartz and MacKinnon, 1997a,b). This rationalization was supported by the experiments shown in Figs. 9–11. Furthermore, we found that the apparent stoichiometry was STX dependent: the greater the STX concentration, the more molecules that appeared to bind per channel. Furthermore, dissociation from the channel was not a first order process. If there were simply n multiple identical sites, the macroscopically observed dissociation would appear first order. These observations all suggests cooperative STX-channel binding and complexity beyond simple binding of ions to multiple identical sites.

STX Stabilizes the Closed State of hERG K^+ Channels

The relationship between membrane potential, channel opening, and STX action can be expressed in terms of an activation energy barrier. If we visualize the outward movement of S4 sensors during channel activation, and that outward movement is facilitated by some negatively charged amino acids lying along the path of S4 sensors or in S3-S4, then shielding negatively charged amino acids by the divalent cationic STX may retard S4 movement and channel opening. We estimated that 10 μM STX stabilized the closed state of the channel by ~3 kcal/mol. Because of this stabilization, a larger membrane potential depolarization was required, in the presence of STX, to overcome this energetic barrier to channel opening. Large depolarizations, e.g., 50 mV, applied to the STX-bound hERG K^+ channel, caused the STX-bound channel to open. The rightward shift in voltage-dependent rate constants that stabilize the closed state, also lead to the accelerated rate of channel closure upon repolarization. The apparent changes in degree of inhibition by different concentrations of STX at different membrane potentials might be explained through changes in affinity. However, there is evidence of continued drug modification of the channels at all potentials, suggesting that the drug is bound.

Conclusions

We conclude that STX modifies the voltage-sensing mechanism of the hERG K^+ channels (activation and inactivation) to retard the channel opening, to slow the rate of channel activation, and to accelerate the rate of channel deactivation. This specific interaction may involve four or more STX molecules per channel acting at extracellular sites, resulting in reduction of hERG K^+ current in steady-state. STX also appears to affect inactivation of the channel through a similar mechanism. The results reveal a novel mechanism for hERG modulation, a novel characteristic of this toxin, and suggest new ways to alter the role these channels play in human myocardial repolarization.

The authors wish to thank Drs. John Imredy, Laszlo Kiss, Ken Koblan, and John Renger for comments, feedback, and suggestions.

Olaf S. Andersen served as editor.

Submitted: 2 March 2003
Revised: 1 May 2003
Accepted: 5 May 2003

REFERENCES

Anumonwo, J.M., J. Horta, M. Delmar, S.M. Taffet, and J. Jalife. 1999. Proton and zinc effects on HERG currents. *Biophys. J.* 77: 282–298.

Armstrong, C.M. 1971. Interaction of tetraethylammonium ion derivatives with the potassium channels of giant axons. *J. Gen. Physiol.* 58:413–437.

Campbell, D.T., and B. Hille. 1976. Kinetic and pharmacological properties of the sodium channel of frog skeletal muscle. *J. Gen. Physiol.* 67:309–323.

Changeux, J.P., and S.J. Edelstein. 1998. Allosteric receptors after 30 years. *Neuron.* 21:959–980.

Chiba, S., and K. Hashimoto. 1969. Ventricular fibrillation induced by saxitoxin into the AV node artery and its prevention by phenoxybenzamine. *Tohoku J. Exp. Med.* 99:103–104.

Evans, M.H. 1969. Mechanism of saxitoxin and tetrodotoxin poisoning. *Br. Med. Bull.* 25:263–267.

Gurrola, G.B., B. Rosati, M. Rocchetti, G. Pimienta, A. Zaza, A. Arcangeli, M. Olivotto, L.D. Possani, and E. Wanke. 1999. A toxin to nervous, cardiac, and endocrine ERG K^+ channels isolated from Centruroides noxius scorpion venom. *FASEB J.* 13:953–962.

Henderson, R., J.M. Ritchie, and G.R. Strichartz. 1973. The binding of labelled saxitoxin to the sodium channels in nerve membranes. *J. Physiol.* 235:783–804.

Ho, W.K., Y.E. Earm, and A.W. Lee. 1998. Voltage dependent block of HERG potassium channels by calcium and magnesium. *J. Physiol.* 507:631–638.

Johnson, J.P., Jr., F.M. Mullins, and P.B. Bennett. 1999a. Human ether-a-go-go-related gene K^+ channel gating probed with extracellular Ca^{2+}. Evidence for two distinct voltage sensors. *J. Gen. Physiol.* 113:565–580.

Johnson, J.P., Jr., J.R. Balser, and P.B. Bennett. 1999b. Enhancement of HERG K^+ currents by Cd^{2+} destabilization of the inactivated state. *Biophys. J.* 77:2534–2541.

Johnson, J.P., Jr., J.R. Balser, and P.B. Bennett. 2001. A novel extracellular calcium sensing mechanism in voltage-gated potassium ion channels. *J. Neurosci.* 21:4143–4153.

Kao, C.Y., and A. Nishiyama. 1965. Actions of saxitoxin on peripheral neuromuscular systems. *J. Physiol.* 180:50–66.

Kao, C.Y. 1966. Tetrodotoxin, saxitoxin and their significance in the study of excitation phenomena. *Pharmacol. Rev.* 18:997–1049.

Kao, C.Y. 1972. Pharmacology of tetrodotoxin and saxitoxin. *Fed. Proc.* 31:1117–1123.

Li-Smerin, Y., and K.J. Swartz. 2000. Localization and molecular determinants of the Hanatoxin receptors on the voltage-sensing domains of a K(+) channel. *J. Gen. Physiol.* 115:673–684.

Li-Smerin, Y., D.H. Hackos, and K.J. Swartz. 2000. A localized interaction surface for voltage-sensing domains on the pore domain of a K+ channel. *Neuron.* 25:411–423.

Lipkind, G.M., and H.A. Fozzard. 1994. A structural model of the tetrodotoxin and saxitoxin binding site of the Na+ channel. *Biophys. J.* 66:1–13.

Mitcheson, J.S., J. Chen, M. Lin, C. Culberson, and M.C. Sanguinetti. 2000. A structural basis for drug-induced Long QT syndrome. *Proc. Natl. Acad. Sci. USA.* 97:12329–12333.

Monod, J., J. Wyman, and J.P. Changeux. 1965. On the nature of allosteric transitions: a plausible model. *J. Mol. Biol.* 12:88–1181.

Mullins, F.M., S.Z. Stepanovic, R.R. Desai, A.L. George, Jr., and J.R. Balser. 2002. Extracellular sodium interacts with the HERG channel at an outer pore site. *J. Gen. Physiol.* 120:517–537.

Numaguchi, H., F.M. Mullins, J.P. Johnson, Jr., D.C. Johns, S.S. Po, I.C. Yang, G.F. Tomaselli, and J.R. Balser. 2000a. Probing the interaction between inactivation gating and d-sotalol block of HERG. *Circ. Res.* 87:1012–1018.

Numaguchi, H., J.P. Johnson, Jr., C.I. Petersen, and J.R. Balser. 2000b. A sensitive mechanism for cation modulation of potassium current. *Nat. Neurosci.* 3:429–430.

Narahashi, T., H.G. Haas, and E.F. Therrien. 1967. Saxitoxin and tetrodotoxin: comparison of nerve blocking mechanism. *Science.* 157:1441–1442.

Narahashi, T. 1972. Mechanism of action of tetrodotoxin and saxitoxin on excitable membranes. *Fed. Proc.* 31:1124–1132.

Noda, M., H. Suzuki, S. Numa, and W. Stuhmer. 1989. A single point mutation confers tetrodotoxin and saxitoxin insensitivity on the sodium channel II. *FEBS Lett.* 259:213–216.

Pardo-Lopez, L., J. Garcia-Valdes, G.B. Gurrola, G.A. Robertson, and L.D. Possani. 2002. Mapping the receptor site for ergtoxin, a specific blocker of ERG channels. *FEBS Lett.* 510:45–49.

Penzotti, J.L., H.A. Fozzard, G.M. Lipkind, and S.C. Dudley, Jr. 1998. Differences in saxitoxin and tetrodotoxin binding revealed by mutagenesis of the Na^+ channel outer vestibule. *Biophys. J.* 75: 2647–2657.

Po, S.S., D.W. Wang, I.C.H. Wang, J.P. Johnson, Jr., L. Nie, and P.B. Bennett. 1999. Modulation of HERG potassium channels by extracellular magnesium and quinidine. *J. Cardiovasc. Pharmacol.* 33:181–185.

Sanchez-Chapula, J.A., and M.C. Sanguinetti. 2000. Altered gating of HERG potassium channels by cobalt and lanthanum. *Pflugers Arch.* 440:264–274.

Sanguinetti, M.C., C. Jiang, M.E. Curran, and M.T. Keating. 1995. A mechanistic link between an inherited and an acquired cardiac arrhythmia: HERG encodes the IKr potassium channel. *Cell.* 81: 299–307.

Satin, J., J.W. Kyle, Z. Fan, R. Rogart, H.A. Fozzard, and J.C. Makielski. 1994. Post-repolarization block of cloned sodium channels by saxitoxin: the contribution of pore-region amino acids. *Biophys. J.* 66:1353–1363.

Scaloni, A., C. Bottiglieri, L. Ferrara, M. Corona, G.B. Gurrola, C. Batista, E. Wanke, and L.D. Possani. 2000. Disulfide bridges of ergtoxin, a member of a new sub family of peptide blockers of the ether a go go related K^+ channel. *FEBS Lett.* 479:156–157.

Silverman, W.R., C.-Y. Tang, A.F. Mock, K.-B. Huh, and D.M. Papazian. 2000. Mg^{2+} modulates voltage-dependent activation in

ether-a-go-go potassium channels by binding between transmembrane segments S2 and S3. *J. Gen. Physiol.* 116:663–677.

Spector, P.S., M.E. Curran, A. Zou, M.T. Keating, and M.C. Sanguinetti. 1996. Fast inactivation causes rectification of the IKr channel. *J. Gen. Physiol.* 107:611–619.

Swartz, K.J., and R. MacKinnon. 1997a. Hanatoxin modifies the gating of a voltage-dependent K+ channel through multiple binding sites. *Neuron.* 18:665–673.

Swartz, K.J., and R. MacKinnon. 1997b. Mapping the receptor site for hanatoxin, a gating modifier of voltage-dependent K+ channels. *Neuron.* 18:675–682.

Trudeau, M.C., J.W. Warmke, B. Ganetzky, and G.A. Robertson. 1995. HERG, a human inward rectifier in the voltage-gated potassium channel family. *Science.* 269:92–95.

Wagner, H.H., and W. Ulbricht. 1976. Saxitoxin and procaine act independently on separate sites of the sodium channel. *Pflugers Arch.* 364:65–70.

Wang, J., M.C. Trudeau, A.M. Zappia, and G.A. Robertson. 1998. Regulation of deactivation by an amino terminal domain in human ether-a-go-go-related gene potassium channels. *J. Gen. Physiol.* 112:637–647.

Wang, S., S. Liu, M.J. Morales, H.C. Strauss, and R.L. Rasmusson. 1997. A quantitative analysis of the activation and inactivation kinetics of HERG expressed in *Xenopus* oocytes. *J. Physiol.* 502:45–60.

Warmke, J.W., and B. Ganetzky. 1994. A family of potassium channel genes related to eag in *Drosophila* and mammals. *Proc. Natl. Acad. Sci. USA.* 91:3438–3442.

Winterfield, J.R., and K.J. Swartz. 2000. A hot spot for the interaction of gating modifier toxins with voltage-dependent ion channels. *J. Gen. Physiol.* 116:637–644.

Wong, J.L., R. Oesterlin, and H. Rapoport. 1971. The structure of saxitoxin. *J. Am. Chem. Soc.* 93:7344–7345.